

## NUMERICAL SOLUTIONS OF 2D AND 3D SLAMMING PROBLEMS

Q Yang and W Qiu, Memorial University of Newfoundland, Canada  
(DOI No: 10.3940/rina.ijme.2011.a2.wf3)

### SUMMARY

Slamming forces on 2D and 3D bodies have been computed based on a CIP method. The highly nonlinear water entry problem governed by the Navier-Stokes equations was solved by a CIP based finite difference method on a fixed Cartesian grid. In the computation, a compact upwind scheme was employed for the advection calculations and a pressure-based algorithm was applied to treat the multiple phases. The free surface and the body boundaries were captured using density functions. For the pressure calculation, a Poisson-type equation was solved at each time step by the conjugate gradient iterative method.

Validation studies were carried out for 2D wedges with various deadrise angles ranging from 0 to 60 degrees at constant vertical velocity. In the cases of wedges with small deadrise angles, the compressibility of air between the bottom of the wedge and the free surface was modelled. Studies were also extended to 3D bodies, such as a sphere, a cylinder and a catamaran, entering calm water. Computed pressures, free surface elevations and hydrodynamic forces were compared with experimental data and the numerical solutions by other methods.

### NOMENCLATURE

$\delta_{ij}$	Kronecker's delta function
$\mu$	Dynamic viscosity ( $\text{N m}^{-2} \text{s}$ )
$\rho$	Density ( $\text{kg m}^{-3}$ )
$\sigma_{ij}$	Total stress ( $\text{N m}^{-2}$ )
$\phi_m$	Density function
$\Omega_m$	Computational domain
$c_s$	Sound speed ( $\text{m s}^{-1}$ )
$C_v$	Ratio of hull velocity
$\hat{f}$	Interpolation function
$P$	Pressure ( $\text{N m}^{-2}$ )
$t$	Time (s)
$u_i$	Velocity ( $\text{m s}^{-1}$ )
$x_i$	Spatial coordinates
2D	Two-Dimensional
3D	Three-Dimensional
CIP	Constrained Interpolation Profile
SPH	Smoothed Particle Hydrodynamics
VOF	Volume of Fluid

However, there are limitations when they are applied to bodies with more complex geometry.

Various numerical methods have been developed to solve the water entry problems based on the potential flow theory. For example, Greenhow [5] used Cauchy's formula to solve the wedge entry problems. In his work, both gravity and nonlinear free surface conditions were taken into account. Zhao and Faltinsen [6] studied the water entry of a wedge using boundary element method with constant elements. The jet tip at the intersection point of the body surface and the free surface was cut and two small constant elements were distributed. Chuang et al. [7] developed a boundary element method based on desingularized Cauchy's formula. A numerical approach was also developed to remove the corner singularity at the intersection point of body surface and free surface.

Although great progress has been made in solving the water entry problem with the potential-flow based methods, it is difficult for these methods to treat highly distorted or breaking free surfaces. These difficulties can be overcome by the computational fluid dynamics (CFD) methods which solve the Navier-Stokes equations. Kleefsman *et al.* [8] have solved the 2D slamming problem of symmetric bodies using the Volume of Fluid (VOF) method and the finite volume discretization on a fixed Cartesian grid. Kim *et al.* [9] used the Smoothed Particle Hydrodynamics (SPH) method to simulate the water entry of 2D asymmetric bodies. Zhu *et al.* [10] studied the water entry and the exit of a horizontal circular cylinder with the Constrained Interpolation Profile (CIP) algorithm in the 2D computational domain. Yang and Qiu [11] solved the 2D water entry problems of symmetric and asymmetric wedges with various deadrise angles using the CIP method. The effect of the compressibility air for small deadrise angles was also discussed in their work in 2008 [12].

### 1. INTRODUCTION

Slamming is a complex nonlinear problem. It has been extensively studied by many researchers with different methods. The theoretical analysis of the similarity flow induced by the wedge entry was first conducted by Wagner [1]. Armand and Cointe [2] and Cointe [3] extended Wagner's theory to analyze the entry problem using matched asymptotic expansions. Furthermore, Dobrovol'skaya [4] developed an analytical solution in terms of a nonlinear singular integral equation for the problem of the symmetrical entry of a wedge into calm water. For wedge-type bodies, these approximate solutions can be used to calculate the slamming forces.

Most of the studies have been focused on solving the 2D water entry problems, and relatively limited attempts have been made to solve the slamming problems of 3D bodies. Shiffman and Spencer [13] developed general expressions for the pressure distributions and slamming forces on a cone. Troesch and Kang [14] computed the slamming forces on a 3D cusped body and a sphere based on the potential flow theory. Faltinsen and Chezhian [15] modelled the water entry of a 3D body using a generalized Wagner method.

In this work, numerical methods have been developed to solve the slamming problems of 2D and 3D bodies with constant water-entry velocities and free-fall motions. The highly nonlinear slamming problems governed by the Navier-Stokes equations are solved by a finite difference method on a fixed Cartesian grid. The free surface is captured with the CIP method. A combined Lagrangian-Eulerian method is applied to model the 2D/3D solid body boundaries. The solid body and free surface interfaces are identified by density functions. The rigid-body motions are described in six degrees of freedom. For the pressure calculation, a Poisson-type equation is solved at each time step by the conjugate gradient iterative method with a Jacobi pre-conditioner. Validation studies have been carried out for 2D and 3D bodies.

## 2. MATHEMATICAL FORMULATIONS

The differential equations governing the compressible and viscous fluid are given as:

$$\frac{\partial \rho}{\partial t} + u_i \frac{\partial \rho}{\partial x_i} = -\rho \frac{\partial u_i}{\partial x_i} \quad (1)$$

$$\frac{\partial u_i}{\partial t} + u_j \frac{\partial u_i}{\partial x_j} = -\frac{1}{\rho} \frac{\partial \sigma_{ij}}{\partial x_j} + f_i \quad (2)$$

where  $t$  is the time;  $x_i$  ( $i=1, 2, 3$ ) are the coordinates in Cartesian coordinate system;  $\rho$  is the mass density;  $u_i$  are the velocity components;  $f_i$  are the body forces.

The equation of state can be written as  $p = f(\rho)$ , where  $p$  is the pressure. Applying the equation of state to Eq. (1) leads to the pressure equation as follows:

$$\frac{\partial p}{\partial t} + u_i \frac{\partial p}{\partial x_i} = -\rho c_s^2 \frac{\partial u_i}{\partial x_i} \quad (3)$$

where  $c_s = \sqrt{\partial p / \partial \rho}$  is the sound speed.

For a Newtonian fluid, the total stress can be written as

$$\sigma_{ij} = -p\delta_{ij} + 2\mu S_{ij} - 2\mu\delta_{ij}S_{kk}/3$$

$$S_{ij} = \frac{1}{2} \left( \frac{\partial u_i}{\partial x_j} + \frac{\partial u_j}{\partial x_i} \right)$$

where  $\mu$  is the dynamic viscosity coefficient and  $\delta_{ij}$  is Kronecker's delta function.

Applying the fractional step approach, the governing Eqs. (1) to (3) can be solved in three steps as follows:

### 1. Advection phase

$$\frac{\partial \rho}{\partial t} + u_i \frac{\partial \rho}{\partial x_i} = 0 \quad (4)$$

$$\frac{\partial u_i}{\partial t} + u_j \frac{\partial u_i}{\partial x_j} = 0 \quad (5)$$

$$\frac{\partial p}{\partial t} + u_i \frac{\partial p}{\partial x_i} = 0 \quad (6)$$

### 2. Non-advection phase I

$$\frac{\partial u_i}{\partial t} = -\frac{2\mu}{\rho} \frac{\partial}{\partial x_j} \left( S_{ij} - \frac{1}{3} \delta_{ij} S_{kk} \right) + f_i \quad (7)$$

### 3. Non-advection phase II

$$\frac{\partial \rho}{\partial t} = -\rho \frac{\partial u_i}{\partial x_i} \quad (8)$$

$$\frac{\partial u_i}{\partial t} = -\frac{1}{\rho} \frac{\partial p}{\partial x_i} \quad (9)$$

$$\frac{\partial p}{\partial t} = -\rho c_s^2 \frac{\partial u_i}{\partial x_i} \quad (10)$$

The advection phase can be computed by the CIP method, developed by Yabe *et al.* [16] based on the work of Yabe *et al.* [17] and Yabe [18]. The non-advection phase I can be solved by the central finite difference method. For the non-advection phase II, a pressure-based algorithm is employed. A Poisson equation can be obtained based on Eq. (9) and Eq. (10):

$$\frac{\partial}{\partial x_i} \left( \frac{1}{\rho^*} \frac{\partial p^{n+1}}{\partial x_i} \right) = \frac{p^{n+1} - p^*}{\rho^* c_s^2 \Delta t^2} + \frac{1}{\Delta t} \frac{\partial u_i^{**}}{\partial x_i} \quad (11)$$

where the superscript \* and \*\* indicate the provisional values before and after the calculations of non-advection phase I. For a perfect incompressible fluid with  $c_s = \infty$ , a simpler Poisson equation can be obtained as follow:

$$\frac{\partial}{\partial x_i} \left( \frac{1}{\rho^*} \frac{\partial p^{n+1}}{\partial x_i} \right) = \frac{1}{\Delta t} \frac{\partial u_i^{**}}{\partial x_i} \quad (12)$$

The conjugate gradient method with the Jacobi pre-conditioner was employed in this work to solve Eq. (12).

In order to identify which part is occupied by water, solid body or air in the computational domain, a density functions  $\phi_m$  is introduced, which satisfies

$$\phi_m(x, y, z, t) = \begin{cases} 1 & (x, y, z) \in \Omega_m \\ 0 & \text{otherwise} \end{cases} \quad (13)$$

where  $\Omega_m$ ,  $m=1, 2$ , and  $3$ , denotes the domain occupied by liquid, solid and air, respectively.

The free surface can be captured by solving the following advection equation with the CIP method:

$$\frac{\partial \phi_1}{\partial t} + u_i \frac{\partial \phi_1}{\partial x_i} = 0 \quad (14)$$

Based on a compact upwind high-order scheme, the density function and its spatial derivatives are used as dependent variables to construct the interface profile. For the 3D problem, a cubic polynomial interpolation function can be constructed in an upwind cell (Fig. 1) based on the work of Yabe [18] as follows:

$$\begin{aligned} \hat{f}_{i,j,k}(x,y,z) = & [(c_1\bar{x} + c_2\bar{y} + c_3\bar{z} + c_4)\bar{x} + c_5\bar{y} + \partial_x f_{i,j,k}] \bar{x} \\ & + [(c_6\bar{y} + c_7\bar{z} + c_8\bar{x} + c_9)\bar{y} + c_{10}\bar{z} + \partial_y f_{i,j,k}] \bar{y} \\ & + [(c_{11}\bar{z} + c_{12}\bar{x} + c_{13}\bar{y} + c_{14})\bar{z} + c_{15}\bar{x} + \partial_z f_{i,j,k}] \bar{z} \\ & + c_{16}\bar{x}\bar{y}\bar{z} + f_{i,j,k} \end{aligned} \quad (15)$$

where  $\bar{x} = -u\Delta t$ ,  $\bar{y} = -v\Delta t$  and  $\bar{z} = -w\Delta t$ , and  $\Delta t$  is the time step. The 16 unknown coefficients are determined from the values of  $f$ ,  $\partial_x f$ ,  $\partial_y f$  and  $\partial_z f$  at grid points  $(i+1, j, k)$ ,  $(i, j+1, k)$  and  $(i, j, k+1)$  and those  $f$  values at points  $(i+1, j+1, k)$ ,  $(i, j+1, k+1)$  and  $(i+1, j+1, k+1)$ .

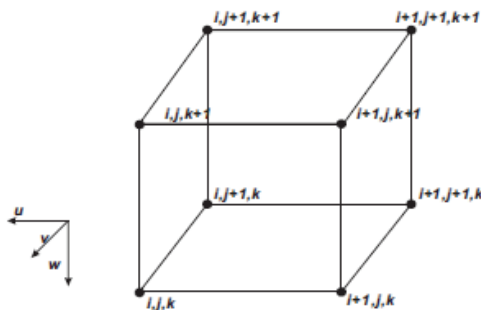


Figure 1: Upwind cubic cell

The combined Euler-Lagrangian method is employed to determine the solid boundary. A body surface is represented by a set of triangular/quadrilateral panels (Fig. 2). Note that small panels need to be concentrated at the corners and locations with large curvature.

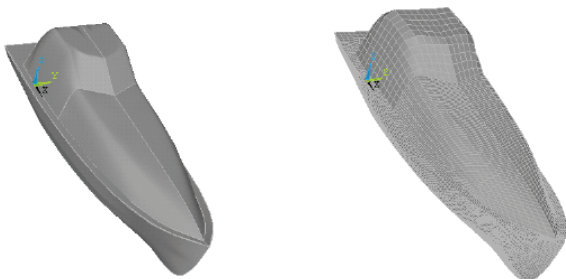


Figure 2: Body geometry and computational model

The density function for solid surface is calculated by:

$$\phi_2 = \sum_{i=1}^{i=N} \varepsilon_i \quad (16)$$

where  $N$  is the number of panels and

$$\varepsilon_i = \int_{\text{panel } i} \bar{F}_i ds \quad (17)$$

The function,  $\bar{F}_i$ , is the distance from a point on the panel  $i$  to the corresponding computational cell surface. The density function for air can then be obtained from  $\phi_3 = 1 - \phi_1 - \phi_2$ . After the density functions for all phases are determined, the physical properties including viscosity and density can be calculated for each computational cell.

Based on the work of Hu and Kashiwagi [19], the force acting on the solid body can be computed by

$$F_i = -\oint_{\Omega} \frac{\partial p}{\partial x_i} \phi_2 d\Omega \quad (18)$$

where  $\Omega$  denotes the whole computational domain and  $\phi_2$  is the density function for solid. After the force and the moment are determined, the motion of the solid body can be solved by the Euler method.

### 3. NUMERICAL RESULTS

#### 3.1 WATER ENTRY OF 2D WEDGES WITH LARGE DEADRISE ANGLES

Computations were first carried out for the symmetric water entry of a wedge tested by Zhao *et al.* [20]. As shown in Fig. 3, the width of the wedge is 0.5m and the maximum drop height is about 2.0m.

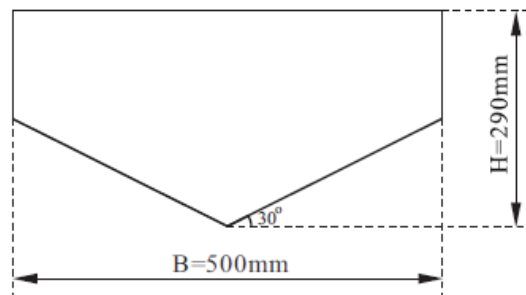


Figure 3: Geometry of wedge section in the drop test

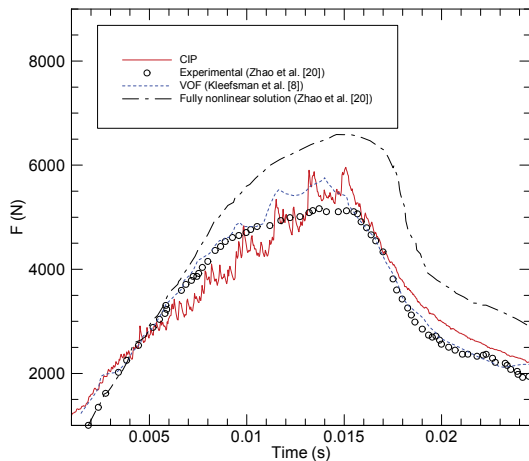
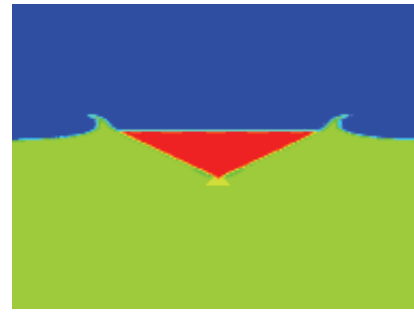


Figure 4: Time history of vertical slamming force

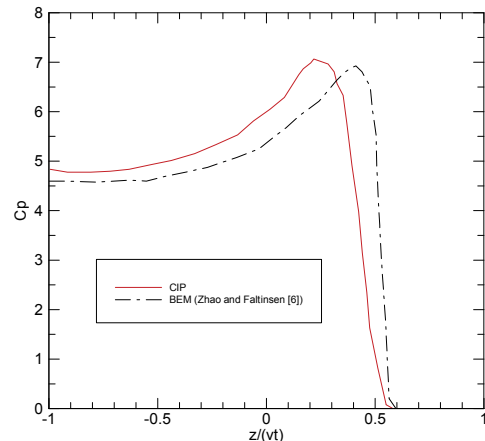
The time history of the computed vertical hydrodynamic force is given in Fig. 4 and compared with the experimental results by Zhao *et al.*, [20], the fully nonlinear solution obtained using the potential flow theory (Zhao *et al.*, [20]), and the numerical solution by the VOF method (Kleefsman *et al.*, [8]). It can be seen that the numerical solutions by the CIP method are in agreement with the experimental results and those by the VOF method.

The computed free surface elevations for the wedge were compared with the test results by Greenhow and Lin [21] in Fig. 5. The visual comparison indicates that the predicted free surface elevations are similar to those shown in the experiments. Pressure distributions on wedges with different deadrise angles were computed and compared with the solutions by the boundary element method (Zhao and Faltinsen [6]) in Fig. 6. Note that the sharp-peaked pressure occurs close to the jet flow area for wedges with smaller deadrise angles. For the wedge with deadrise angle of  $60^\circ$ , the maximum pressure point tends to move to the keel of the wedge. The value of maximum pressure drops quickly for wedges with larger deadrise.

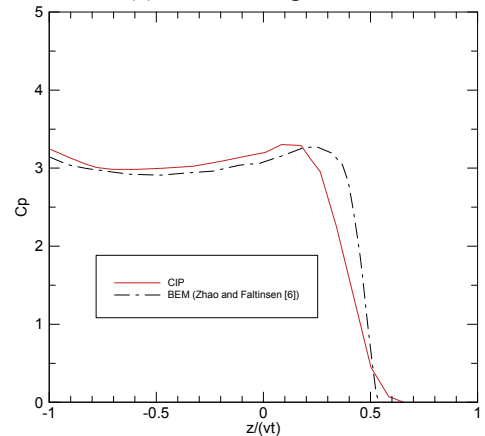


(b) Computed

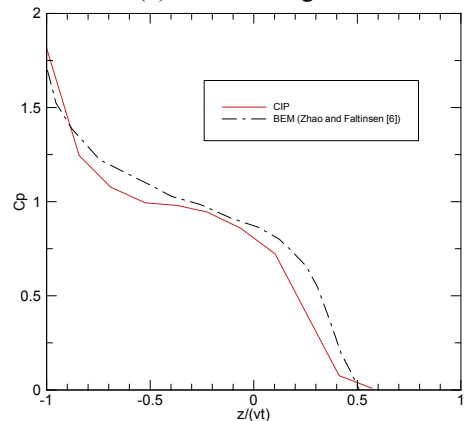
Figure 5: Comparison of free surface elevations



(a) Deadrise angle= $30^\circ$



(b) Deadrise angle= $40^\circ$



(c) Deadrise angle= $60^\circ$

Figure 6: Pressure distribution on wedges with different deadrise angles



(a) Experimental (Greenhow and Lin, [21])

### 3.2 WATER ENTRY OF 2D WEDGES WITH SMALL DEADRISE ANGLES

The numerical method has also been used to solve the water-entry problems for wedges with small deadrise angles. In the computation, the compressible air was considered.

Computations were carried out for a plate entering calm water and the numerical solutions were compared with the experimental results by Verhagen [22]. The plate was 0.4m in width and entered the water at a constant velocity of 2.8m/s. A pressure transducer was placed at the centre of the plate for pressure measurement. Figure 7 shows the time history of the non-dimensional pressure ( $P/P_0$ ) with  $P_0 = 10^5$  Pa and its comparison with the experimental results. The comparison with experimental data shows good agreement, especially for the peak pressure. Figure 8 presents the compressible air flow between the plate and water surface. Before the plate bottom touched the free surface, a compressible air layer was developed between the plate and the water surface, and the air moved away from the two edges of the plate. An air cushion was formed between the plate and the free surface.

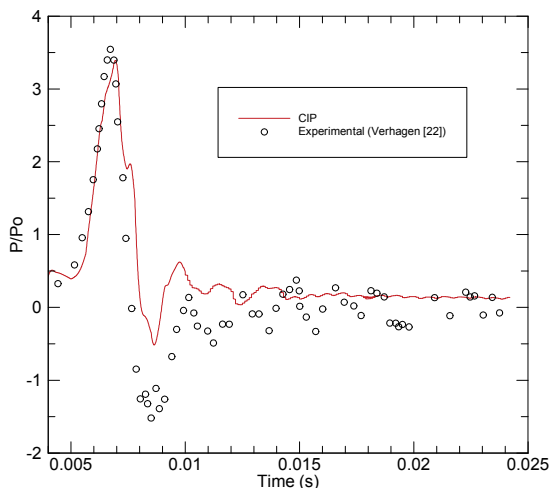


Figure 7: Pressure during the water entry of a plate

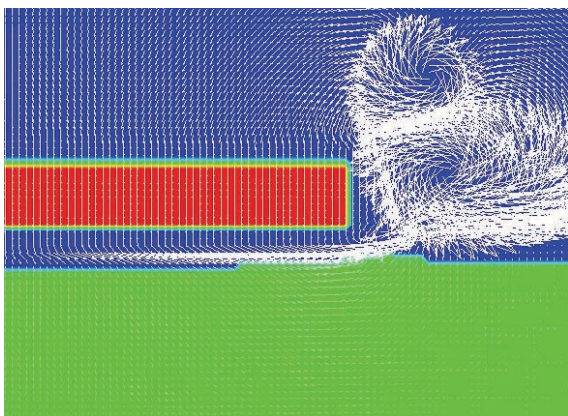


Figure 8: Air flow between the plate and water surface

The computations have been extended to a series of wedges with small deadrise angles by considering the compressible air. The computed maximum pressures are given in Fig. 9 and compared with the experimental results by Chuang [23] and those by the Wagner theory. It can be seen that the Wagner theory gives extremely large pressure for small deadrise angles and infinite pressure at  $0^\circ$  deadrise angle. The numerical results by the CIP method are in a good agreement with Chuang's experimental results.

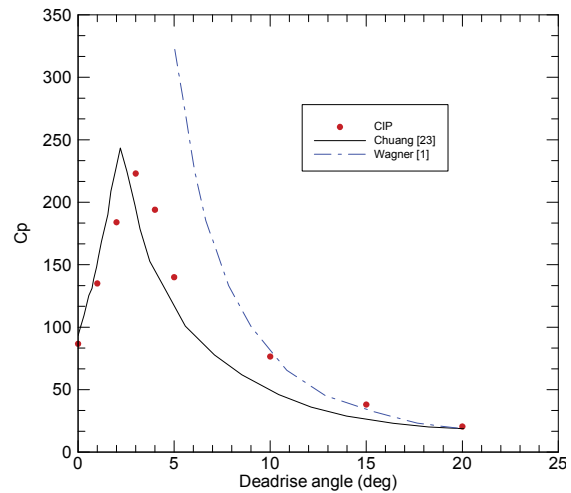


Figure 9: Maximum pressures for wedge with small deadrise angles

### 3.3 WATER ENTRY OF SPHERE WITH CONSTANT DROP VELOCITY

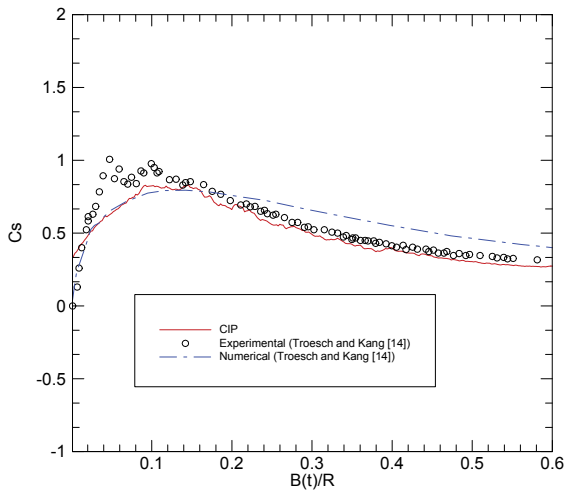
The water entry of a sphere subjected to oblique impact angles was studied in this work. Model tests were carried out by Troesch and Kang [14] for a sphere entering calm water with both vertical and horizontal velocities. The diameter of the sphere was 0.502m. The sphere was dropped from a moving carriage with a speed corresponding to the vertical impact velocity, which resulted in an oblique entry angle of 45 degrees.

Computations were carried out for two drop heights, 0.61m and 1.22m, which corresponded to impact velocities of 2.46m/s and 4.89m/s, respectively. The surface of the sphere was represented by 200 triangular panels and 19,800 rectangular panels in the computation. The computational grid was  $178 \times 178 \times 178$  and the time step was chosen as  $1.027 \times 10^{-4}$  s. The non-dimensional slamming coefficient is defined as

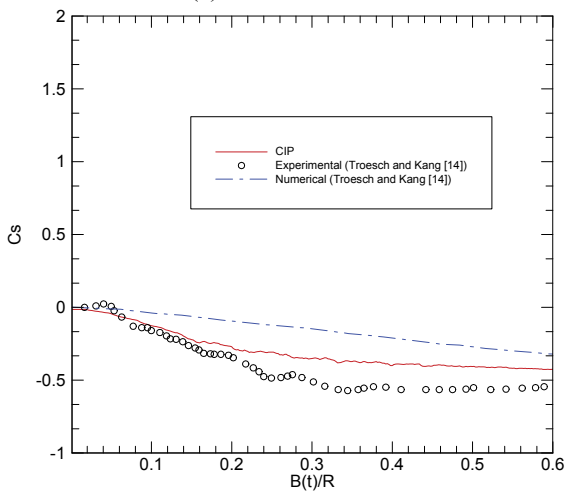
$$C_s = \frac{F_I}{\frac{1}{2} \rho \pi R^2 V^2}$$

where  $F_I$  is the vertical or horizontal impact force,  $V_0$  is the initial impact velocity, and  $R$  is the radius of the sphere. The computed horizontal and vertical slamming coefficients are compared with the experimental results

in Figs. 10 and 11 and the numerical solutions based on the potential flow theory (Troesch and Kang [14]).

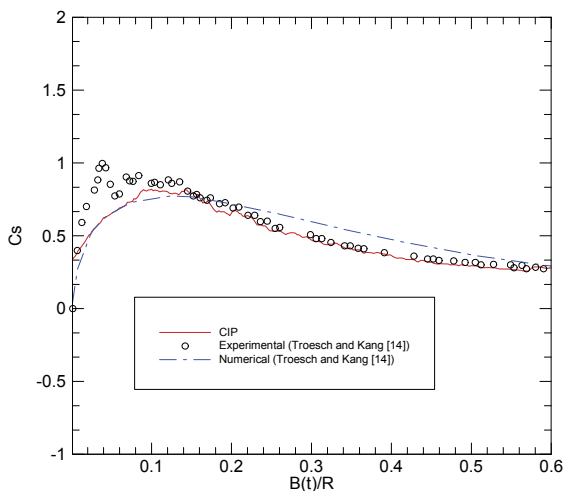


(a) Vertical forces

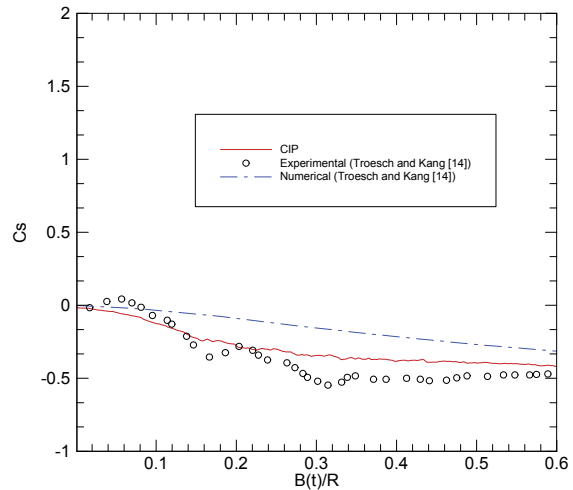


(b) Horizontal forces

Figure 10: Slamming force on a sphere (drop height=0.61m)



(a) Vertical forces



(b) Horizontal forces

Figure 11: Slamming force on a sphere (drop height=1.22m)

In these figures,  $B(t)$  is the instantaneous submerged depth of sphere. As shown, the numerical solutions by the 3D CIP method are generally in a better agreement with experimental results in comparison with numerical solutions by the potential flow theory.

### 3.4 WATER ENTRY OF 3D CATAMARAN WITH FREE-FALL MOTION

The water entry of a catamaran with free-fall motion was computed with the CIP method. The catamaran hull experiences cross-deck slamming during the water entry. A model drop test was carried out for a segment of catamaran hull by Davis and Whelan [24]. The model was 0.544m wide and 0.5m long, and the geometry of cross section is shown in Fig. 12. In the computation, the model was represented by 8,598 panels. The computational grid was  $98 \times 98 \times 88$  and the time step was chosen as  $1.84 \times 10^{-4}$  s.

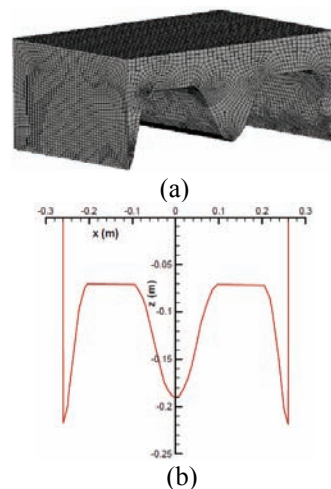
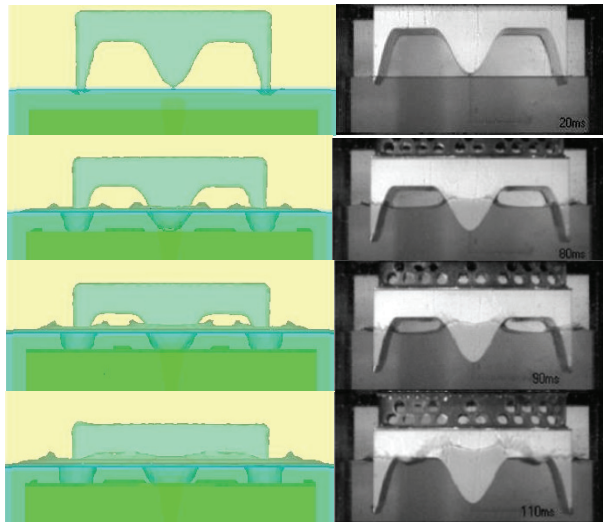


Figure 12: Computational model of catamaran and the cross section

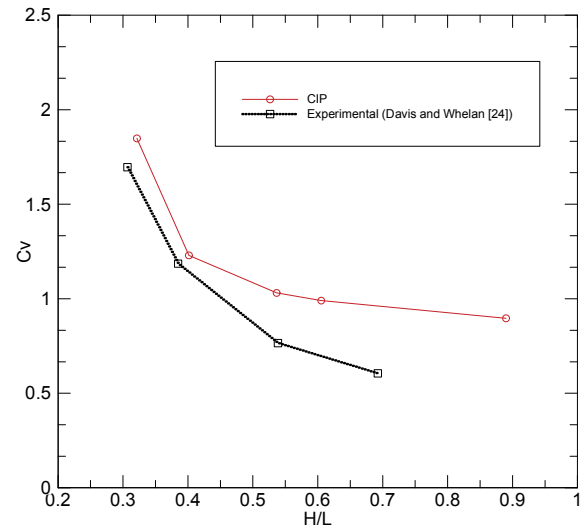
There were two main parameters used in the drop tests, the nondimensional drop height ( $H/L$ ) which defines the maximum velocity just prior to the water entry and the mass ratio  $m^* = m_m / \rho T L^2$ , where  $H$  is the drop height from the water surface to the top of the wet deck when the model is released,  $L$  is the overall width (0.544 m) of the model,  $m_m$  is the model mass,  $\rho$  is the water density and  $T$  is the length of the model (0.5 m). Note that the velocity of a large mass ratio model is not greatly reduced when the model enters water. A small mass ratio model leads to a greater velocity reduction.



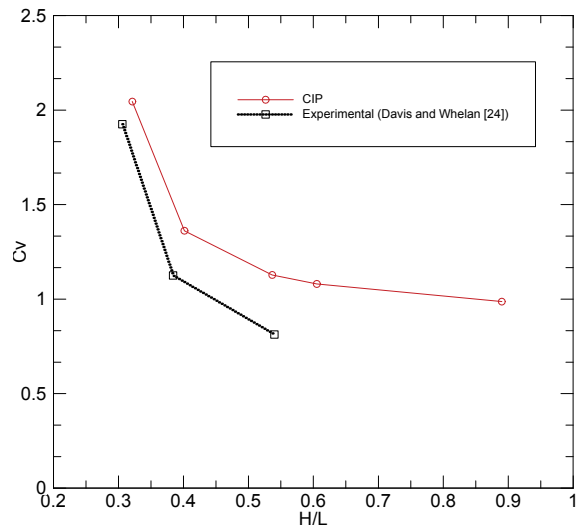
(a) Computed (b) Experimental  
Figure 13: Comparison of free surface elevations

The computed free surface elevations for catamaran were compared with the test results by Davis and Whelan [24] in Fig. 13. The visual comparison indicates that the predicted free surface elevations are larger than those observed in the experiments.

The ratios of hull velocity  $C_v$ , defined as the velocity at the time when the top of the wet deck arch touches the initial water level to the velocity at initial water contact, at various drop heights are compared with the experimental data in Fig. 14. The comparison was made for two mass ratios,  $m^*=0.29$  and  $0.58$ . As shown in the figure, the trend of the predicted values is in an agreement with that of the experimental data, while the CIP method over-predicted the velocity ratios, especially for large drop heights. Note that the compressibility of air was not taken into account in the computations, which likely led to the over-prediction.



(a)  $m^*=0.29$   
(b)

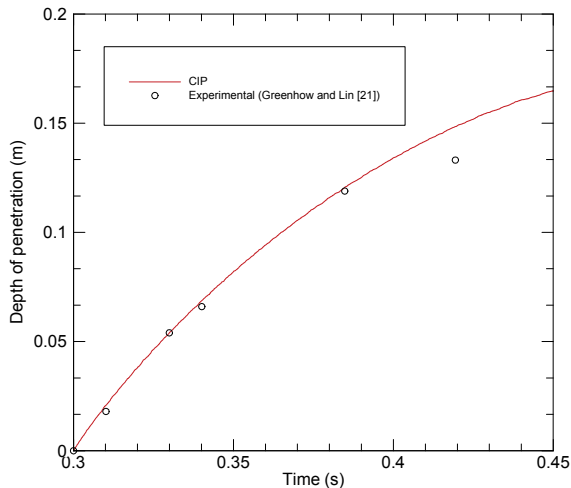


(c)  $m^*=0.58$

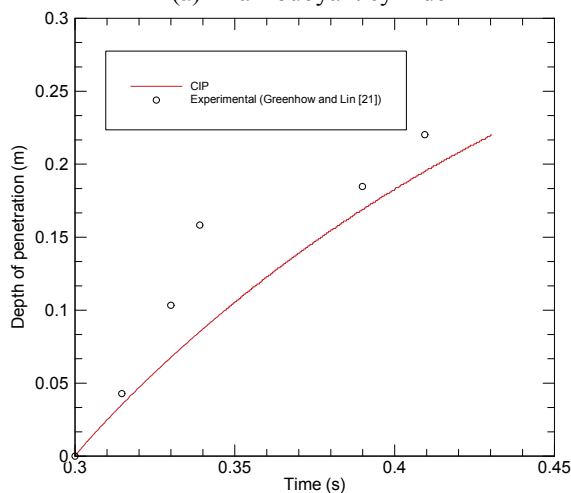
Figure 14: Velocity ratios for the catamaran model

### 3.5 WATER ENTRY OF 3D CYLINDER WITH FREE-FALL MOTION

Computations were also carried out for the free fall of 3D cylinders entering calm water. A half-buoyant and a neutrally buoyant cylinder of 0.055m in radius and 1m in length were used in the validation studies. The computational grid was  $178 \times 78 \times 158$  and the time step was chosen as  $1.02 \times 10^{-3}$ s. The cylinder was dropped from a height of 0.5m between the lowest point of the cylinder and the undisturbed free surface. Numerical results are compared with the experimental results by Greenhow and Lin [21].



(a) Half-buoyant cylinder



(b) Neutrally buoyant cylinder

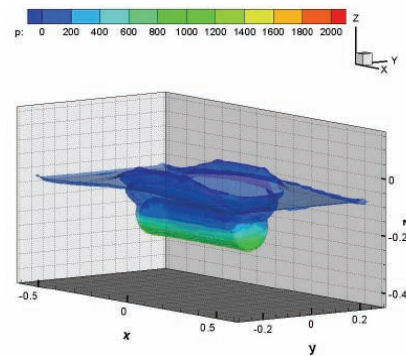
Figure 15: Depth of penetration during water entry of cylinders

Figure 15 presents the time history of the depth of penetration for the half-buoyant and neutrally buoyant cylinders. For the half-buoyant cylinder, there is a good agreement between the numerical results and experimental data. For the neutrally buoyant cylinder, the CIP method under-predicted the depth of penetration. Figure 16 shows pressure distributions of the neutrally buoyant cylinder and the half-buoyant cylinder at the same time instant. As expected, the maximum pressure on the bottom of the neutrally buoyant cylinder is larger than that of the half-buoyant cylinder.

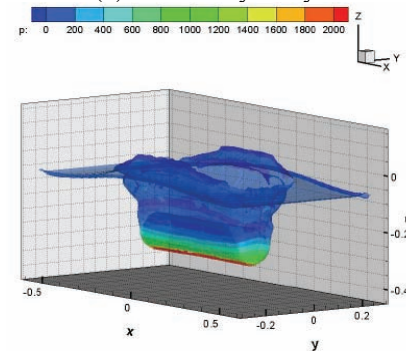
#### 4. CONCLUSIONS

A numerical method was developed to compute the slamming forces on 2D and 3D bodies entering calm water. The multiphase problem governed by Navier-Stokes equations was solved by a CIP based finite difference method on a fixed Cartesian grid. The nonlinear free surface was captured by the CIP method. Slamming forces, pressure distribution, free surface deformation, and motion of body were predicted.

Validation studies were carried out for 2D and 3D bodies. It has been demonstrated that the CIP method is robust and reliable to solve the slamming problems of bodies entering calm water with constant velocity or free-fall motion.



(a) Half-buoyant cylinder



(b) Neutrally buoyant cylinder

Figure 16: Pressure distribution on cylinders

#### 5. ACKNOWLEDGEMENTS

This work was supported by the Natural Sciences and Engineering Research Council (NSERC) of Canada, Defence Research and Development Canada Atlantic and Oceanic Consulting Corporation through a partnership program.

#### 6. REFERENCES

1. WAGNER, H., 'Über Stoss und Gleitvorgänge an der Oberfläche von Flüssigkeiten', Zeitschrift für Angewandte Mathematik und Mechanik, Vol. 12, No. 4, pp. 193-235, 1932.
2. ARMAND, J.L. and COINTE, R., 'Hydrodynamic Impact Analysis of a Cylinder', Proceedings of the Fifth International Offshore Mechanics and Arctic Engineering, Tokyo, Japan, Vol. 1, pp. 609-634, 1986.
3. COINTE, R., 'Free Surface Flows Close to a Surface-Piercing Body', Mathematical Approaches in Hydrodynamics (ed. T. Miloh), Soc. Ind. Appl. Maths, Philadelphia, pp. 319-334, 1991.

4. DOBROVOL'SKAYA, Z.N., 'On Some Problems of Similarity Flow of Fluid with a Free Surface', *Journal of Fluid Mechanics*, Vol. 36, pp. 805-829, 1969.
5. GREENHOW, M., 'Wedge Entry into Initially Calm Water', *Applied Ocean Research*, Vol. 9, pp. 214-223, 1987.
6. ZHAO, R. and FALTINSEN, O., 'Water Entry of Two-Dimensional Bodies', *J. Fluid Mech.*, Vol. 246, pp. 593-612, 1993.
7. CHUANG, J.M., ZHU, W. and QIU, W., 'Numerical Solutions of 2D Water Entry Problem', *Proceedings of ISOPE2006, San Francisco*, 2006.
8. KLEEFMAN, K.M.T., FEKKEN, G., VELDMAN, A.E.P., IWANOWSKI, B. and BUCHNER, B., 'A Volume-of-Fluid Based Simulation Method for Wave Impact Problems', *Journal of Computational Physical*, Vol. 206, pp. 363-393, 2005.
9. KIM, Y.W., KIM, Y., LIU, Y.M., and YUE, D.K.P., 'On the Water-Entry Impact Problem of Asymmetric Bodies', *Proceedings of 9th International Conference on Numerical Ship Hydrodynamics, Ann Arbor, Michigan*, 2007.
10. ZHU, X., FALTINSEN, O. M. and HU, C., 'Water Entry and Exit of a Horizontal Circular Cylinder', *24th International Conference on Offshore Mechanics and Arctic Engineering, Halkidiki, Greece*, 2005.
11. YANG, Q. and QIU, W., 'Numerical Solution of 2D Slamming Problem with a CIP Method', *International Conference on Violent Flows, VF-2007, Research Institute for Applied Mechanics, Kyushu University, Japan*, 2007.
12. YANG, Q. and QIU, W., 'Computation of Slamming Forces on Wedges of Small Deadrise Angles Using a CIP Method', *Proceedings of the 18th International Offshore and Polar Engineering Conference, Vancouver, Canada*, 2008.
13. SHIFFMAN, M. and SPENCER, D.C., 'The Force of Impact on a Cone Striking a Water Surface', *Communications on Pure and Applied Mathematics*, Vol. 4, pp. 379-417, 1951.
14. TROESCH, A.W. and KANG, C.G., 'Hydrodynamic Impact Loads on 3-D Bodies', *Symposium on Naval Hydrodynamics, University of California, Berkeley*, 1986.
15. FALTINSEN, O.M. and CHEZHIAN, M., 'A Generalized Wagner Method for Three-Dimensional Slamming', *Journal of Ship Research*, Vol. 49, No. 4, pp. 279-287, 2005.
16. YABE, T., XIAO, F. and UTSUMI, T., 'The Constrained Interpolation Profile Method for Multiphase Analysis', *Journal of Computational Physics*, Vol. 169, pp. 556-593, 2001.
17. YABE, T., ISHIKAWA, T, WANG, P.Y., AOKI, T., KADOTA, Y. and IKEDA, F., 'A Universal Solver for Hyperbolic Equations by Cubic Polynomial Interpolation II. Two- and Three- Dimensional Solvers', *Computer Physics Communication*, Vol. 66, pp. 233-242, 1991.
18. YABE, T., 'A Universal Cubic Interpolation Solver for Compressible and Incompressible Fluids', *Shock Waves*, Vol. 1, pp. 187-195, 1991.
19. HU, C. and KASHIWAGI, M., 'A CIP-Based Method for Numerical Simulations of Violent Free-Surface Flow', *J. Mar. Sci. Tech.*, Vol. 9, pp. 143-157, 2004.
20. ZHAO, R., FALTINSEN, O. and AARSNES, J., 'Water Entry of Arbitrary Two-Dimensional Sections with and without Flow Separation', *Proceedings of 21st Symposium on Naval Hydrodynamics, Trondheim, Norway*, 1996.
21. GREENHOW, M. and LIN, W.M., 'Nonlinear Free Surface Effects: Experiments and Theory', *Report No. 83-19, Department of Ocean Engineering, MIT, Cambridge, MA*, 1983.
22. VERHAGEN, J.H.G., 'The Impact of a Flat Plate on a Water Surface', *Journal of Ship Research*, Vol. 11, No.4, Dec. 1967.
23. CHUANG, S.L., 'Experimental on Slamming of Wedge-Shape Bodies', *Journal of Ship Research*, Vol. 11, pp. 190-198, 1967.
24. DAVIS, M.R. and WHELAN, J.R., 'Computation of Wet Deck Bow Slam Loads for Catamaran Arched Cross Sections', *Ocean engineering*, 2007.